Magnetic Resonance in Medicine 50:1199–1208 (2003)

Quantitative Assessment of Carotid Plaque Composition Using Multicontrast MRI and Registered Histology

Sharon E. Clarke,[1,2] Robert R. Hammond,[3,4] J. Ross Mitchell,[5,6] and Brian K. Rutt[1,2*]

MRI is emerging as a promising modality for monitoring carotid atherosclerosis. Multiple MR contrast weightings are required for identification of plaque constituents. In this study, eight MR contrast weightings with proven potential for plaque characterization were used to image carotid endarterectomy specimens. A classification technique was developed to create a tissue-specific map by incorporating information from all MR contrast weightings. The classifier was validated by comparison with micro-CT (calcification only) and with matched histological slices registered to MR images using a nonlinear warping algorithm (other components). A pathologist who was blinded to the classifier results manually segmented digitized histological images. The sensitivity of the classifier, as determined by pixel-by-pixel comparison with the pathologist's segmentation and micro-CT, was 60.4% for fibrous tissue, 83.9% for necrosis, 97.6% for calcification, and 65.2% for loose connective tissue. The corresponding values for specificity were 87.9%, 75.0%, 98.3%, and 94.9%, respectively. In conclusion, multicontrast MRI was successfully used in conjunction with a supervised classification algorithm to identify plaque components in endarterectomy specimens. Furthermore, this methodology will provide a framework for comparing different classification algorithms, and determining which combination of MR contrasts will be most valuable for in vivo plaque imaging. Magn Reson Med 50:1199–1208, 2003. © 2003 Wiley-Liss, Inc.

Key words: carotid artery; atherosclerosis; histology; multicontrast; segmentation

Atherosclerosis is a chronic and progressive disease that is characterized by the accumulation of lipids and fibrous tissue within the artery wall (1). Disruption of atherosclerotic plaques at the carotid bifurcation is believed to be the underlying cause of many embolic strokes; furthermore, the histological composition of carotid atheroma is related to a plaque's vulnerability to rupture (2,3). In general, unstable plaques are characterized by a thin, fibrous cap that separates a pool of extracellular lipid and necrosis from the lumen (4). If the integrity of the fibrous cap is compromised, the necrotic core is exposed to the bloodstream and thrombus formation may occur. Several factors may play a role in triggering plaque rupture, including the size and spatial distribution of various plaque components (5); however, the specific plaque components or mechanisms responsible for plaque rupture and/or erosion and subsequent clinical events have yet to be elucidated (4). Further knowledge regarding the explicit features that confer vulnerability to a lesion may come from studies that track changes in plaque composition over time.

MR is a promising noninvasive technique for characterizing atherosclerotic plaque composition. Because of the complexity and variability of atherosclerotic lesions, it is necessary to employ several MR contrast weightings to adequately discriminate between plaque constituents. Ex vivo studies have demonstrated that T_2-weighted contrast alone is inadequate for measuring the size of the lipid core (6), but a combination of proton density, partial T_2, T_2, and diffusion-weighted spin-echo sequences can provide a more accurate assessment of plaque microstructure (7). Multicontrast-weighted MR has also been shown to be necessary for characterizing plaque in vivo. In a series of patients undergoing carotid endarterectomy, no single MR contrast weighting was able to identify lipid-rich necrotic cores and intraplaque hemorrhage; rather, a review of proton density, T_1, T_2, and time-of-flight (TOF) contrast weightings was required (8). In a subsequent investigation, these same four contrast weightings provided enough information to successfully classify carotid plaques according to a modified American Heart Association classification scheme (9). These studies have firmly established the need for multiple contrast weightings in assessing plaque composition; however, in most cases the MR images required interpretation by a trained observer, and thus classification results were subject to variability. Clearly, the development of an algorithm to quantitatively integrate information obtained from multiple MR acquisitions would facilitate accurate and reproducible assessment of plaque composition. This would be advantageous for any study in which the primary aim is to detect changes in plaque composition and morphology over time.

The purpose of the present study was to develop a technique that incorporated information from multicontrast MR images to create a single classified map of plaque components, and then validate the classifier results by comparison with corresponding histology. The accuracy of the classified image was determined by comparing the results with CT images (calcification only) and a pathologist's interpretation of the histology (other components). Accuracy assessment was facilitated by registering the MR images with corresponding histology using a nonlinear warping algorithm, thereby permitting a pixel-by-pixel

[1]Imaging Research Laboratories, Robarts Research Institute, London, Canada.

[2]Department of Medical Biophysics, University of Western Ontario, London, Canada.

[3]Department of Pathology, University of Western Ontario, London, Canada.

[4]Department of Clinical and Neurological Sciences, London Health Sciences Centre, London, Canada.

[5]Department of Radiology, Seaman Family MR Research Centre, Foothills Medical Centre, University of Calgary, Alberta, Canada.

[6]Department of Clinical Neurosciences, Seaman Family MR Research Centre, Foothills Medical Centre, University of Calgary, Alberta, Canada.

Grant sponsor: Canadian Institutes of Health Research; Grant number: GR-14973; Grant sponsors: Barnett-Ivey-Heart and Stroke Foundation of Ontario; MS Society of Canada; Alberta Heritage Foundation for Medical Research.

*Correspondence to: Brian K. Rutt, Imaging Research Laboratories, Robarts Research Institute, P.O. Box 5015, 100 Perth Drive, London, Ontario N6A 5K8, Canada. E-mail: brian.rutt@imaging.robarts.ca

Received 14 April 2003; revised 7 July 2003; accepted 27 July 2003.

DOI 10.1002/mrm.10618

Published online in Wiley InterScience (www.interscience.wiley.com).

Table 1
Acquisition Parameters

	Pdw FSE	Partial T2 FSE	T2w FSE	T1w FSE	FIESTA	T1w SPGR	SGPR MT	Dw SE
TR (ms)	2000	2000	2000	500	5.3	35	35	2000
TE (ms)	7.8	32	62	7.8	2.5	5.9	5.9	25
ETL[a]	8	8	8	8	–	–	–	–
FOV[b] (cm)	2	2	2	2	2	8	8	4
Matrix	128 × 128	128 × 128	128 × 128	128 × 128	128 × 128	512 × 512	512 × 512	256 × 256
Thickness (mm)	0.5	0.5	0.5	0.5	0.2	1	1	1
Slice gap (mm)	0.5	0.5	0.5	0.5	0	0	0	0
Bw[c] (kHz)	±32	±32	±32	±32	±15.6	±15.6	±15.6	±15.6
NEX[d]	16	16	16	21	6	1	1	2
Flip angle	90	90	90	90	35	25	25	90
Other							MT	b = 1500 s/mm^2

[a]ETL, echo train length.
[b]FOV, field of view.
[c]Bw, Bandwidth.
[d]NEX, number of excitations.

comparison of the classifier results with histology. This technique provided a framework for precisely evaluating classifier accuracy, because in addition to the presence or absence of a particular plaque constituent, the size and spatial distribution of each component were considered.

METHODS

MRI

Eight carotid endarterectomy specimens were obtained from surgery, stored at −80°C, and then rewarmed to 37°C prior to and during imaging. The specimens were imaged on a 1.5 T GE CV/i scanner with a custom-built 2-cm-diameter solenoid radiofrequency (RF) coil. A custom-made gradient insert coil interfaced to the clinical scanner allowed a maximum gradient strength of 200 mT/m and a slew rate of 750 T/m/s. The endarterectomy specimens were maintained at 37°C by the use of a heat gun that circulated warm air around the mounted specimen. The specimens were immersed in freon oil (Halocarbon Products Corp., River Edge, NJ). This fluid has no MR signal, so the boundary between lumen and plaque was easily delineated (10).

Eight different MR contrasts were obtained: proton density-weighted (PDw), T_2-weighted (T_2w), and T_1-weighted (T_1w) fast spin echo (FSE), fast imaging employing steady-state acquisition (FIESTA), T_1-weighted spoiled gradient-echo (T_1w SPGR), T_1w SPGR with magnetization transfer (MT), and diffusion-weighted (Dw) (b = 1500 s/mm^2) spin echo (SE). The in-plane resolution for all acquisitions was 156 μm × 156 μm, and the slice thickness varied from 200 to 1000 μm. For all acquisition parameters, see Table 1. The total imaging time per endarterectomy sample was approximately 2 hr; however, the quality of the resulting histological sections was not significantly compromised.

CT Imaging

Following MR scanning, the specimens were fixed in formalin, mounted in a custom-designed holder, and imaged with micro-CT (μCT) at 80 kVp with 52 μm isotropic resolution (MS-8X-90 scanner; General Electric Medical Systems). A cortical bone-mimicking substance (SB3; Gammex RMI, Middleton, WI) was placed alongside the specimen and included in the imaging volume. SB3 has been shown to have properties similar to cortical bone over a wide range of x-ray energies (11). Because calcium is removed during histological processing, the μCT images served as the gold standard for identifying calcium deposits within the atherosclerotic plaque.

Histological Preparation

After imaging, the endarterectomy specimens were decalcified, embedded in paraffin, and then sectioned and stained with Movat's pentachrome and hematoxylin and eosin (H&E) at 0.5-mm intervals. Digital images of the histological preparations were acquired at either 39- or 25-μm in-plane resolution, depending on the size of the plaque. Histology served as the gold standard for all plaque components apart from calcification.

Image Processing

The MR images were manipulated using ImageJ software (12) (National Institutes of Health) so that a stack of images was created for each slice location, i.e., for a slice at a given location through the endarterectomy sample, a file was created that contained the eight MR acquisitions (PDw, partial T_2w, T_2w, T_1w, FIESTA, T_1w SPGR, T_1w SPGR with MT, and Dw) in the order in which they were acquired. These image stacks were then imported into an IDL-based image processing software program (Research Systems Inc., Boulder, CO) for further analysis.

Histological slides were matched with MR images at the same location. Slices were matched by observing the overall morphology of the plaque, as well as the known distance of each slice from the common carotid bifurcation. Similarly, the most appropriate μCT slice was selected by visual comparison to the MR images.

Carotid Plaque Classification

We chose to segment the MR images using the minimum distance to means classifier (henceforth referred to as the

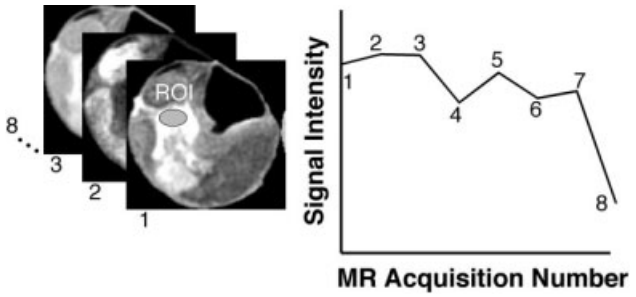

FIG. 1. Schematic of the methods. The classifier was trained by selecting small ROIs representative of each tissue class, and then recording the mean signal intensity of the ROI on each of the eight different MR contrast weightings. The figure illustrates this procedure for one ROI for one plaque. By averaging these values for several ROIs on different plaques, a characteristic signature for each plaque component was calculated.

minimum distance classifier), a supervised classification algorithm. Supervised classification techniques require user input to select a small number of representative pixels for each class (in this case, a class represents a plaque component), referred to as training data. In the case of the minimum distance classifier, the mean signal intensity on each MR contrast weighting is estimated from the training data for each class. The algorithm then calculates the Euclidean distance of each pixel from the mean vector for each class and assigns the pixel to the nearest class (13).

The range of signal intensities in the MR images varied greatly between MR contrast weightings. Preliminary attempts at plaque classification that used the raw signal intensities in the MR images yielded very poor results. The classifier performance was inadequate because contrast weightings with high average signal intensity dominated the classification results, but these contrast weightings did not necessarily have the highest image contrast between plaque components of interest. In order to give all eight contrast weightings equal influence in the minimum distance classifier, each image was normalized prior to selection of training data so that the range of grayscale values in the image was between 0 and 1000.

From the eight endarterectomy specimens imaged, 10 individual cross sections containing atherosclerotic plaques were selected for analysis. Using histology as a guide, training regions were selected for all 10 plaques. The number of pixels in the training regions for each tissue type was as follows: fibrous tissue (1075 pixels pooled from 10 plaques), necrotic (999 pixels from 10 plaques), loose connective tissue (359 pixels from three plaques), and calcification (475 pixels from seven plaques). Some studies have also included hemorrhage as a plaque component; however, we did not do so because there were no substantial examples of hemorrhage in our sample of endarterectomy specimens. The signal intensity for the training regions on each MR contrast weighting was recorded (Fig. 1). These values were then averaged to determine the mean signal intensity as a function of MR acquisition type for each plaque component. Using the information derived from the training regions, the minimum distance classification algorithm was applied to all 10 plaques in the data set.

Image Registration

Histological slides corresponding to the MR slice locations were digitized and then registered to the MR images within the IDL software environment. Thirty to 60 user-defined homologous points were selected, using the lumen and outer plaque boundaries. Obvious internal plaque features, such as large areas of calcification, were also used to select homologous points. Once these points were chosen, the histology was warped to match the MR image by use of the Delaunay triangle method. Delaunay triangle warping fits triangles to irregularly spaced registration points and interpolates values to the output grid. The registration between MR and histology was completed prior to the minimum distance segmentation of the MR images and the interpretation of the histology by the pathologist, thereby eliminating any bias.

The μCT images were registered to the MR images by scaling, translation, and rotation transformation only. The ImageJ plug-in Align 3TP was used for this registration. The scaling factor was known from the relative sizes of the μCT and MR pixels. Translation and rotation were obtained by using Align 3TP plug-in to match the orientation of a user-defined straight line that was drawn on both the μCT and MR images.

Validation of the Classifier

A pathologist who was blinded to the appearance of the MR images and the results of the classifier manually segmented the digitized histological images into regions of fibrous tissue, necrotic core, and loose connective tissue. These tissue classes were clearly defined prior to classification as follows: regions of densely packed collagen were termed fibrous; areas containing acellular debris (amorphous material with or without cholesterol crystals) were called the necrotic core. If a region consisted of >50% space due to the presence of blood vessels and/or collagen strands in a reticular arrangement, it was termed loose connective tissue. Photomicrographs representative of each tissue class are shown in Fig. 2. The pathologist assessed plaque composition by examining the slide under the microscope, and outlining and labeling corresponding regions on the digitized image. The digitized image was displayed in Adobe Photoshop (version 7, Adobe Systems Inc., CA), and the various plaque components were outlined with a drawing tablet (Graphire2; Wacom Technology Corporation, WA). The digitized histological image, including the pathologist's tracings, was warped to match the MR image by use of the nonlinear warping algorithm described in the previous section. Regions identified by the pathologist as belonging to a specific plaque constituent served as "truth regions" against which the minimum distance classifier results were validated. The pathologist was instructed to identify fibrous tissue, necrosis, and loose connective tissue only, and to ignore regions of calcification. The pathologist attempted to divide the entire plaque cross section into regions that could be identified as one of the three plaque components; therefore, the truth regions were much larger than the training regions. The training regions comprised only 4% of the total number of pixels analyzed. Although the pathologist did not select

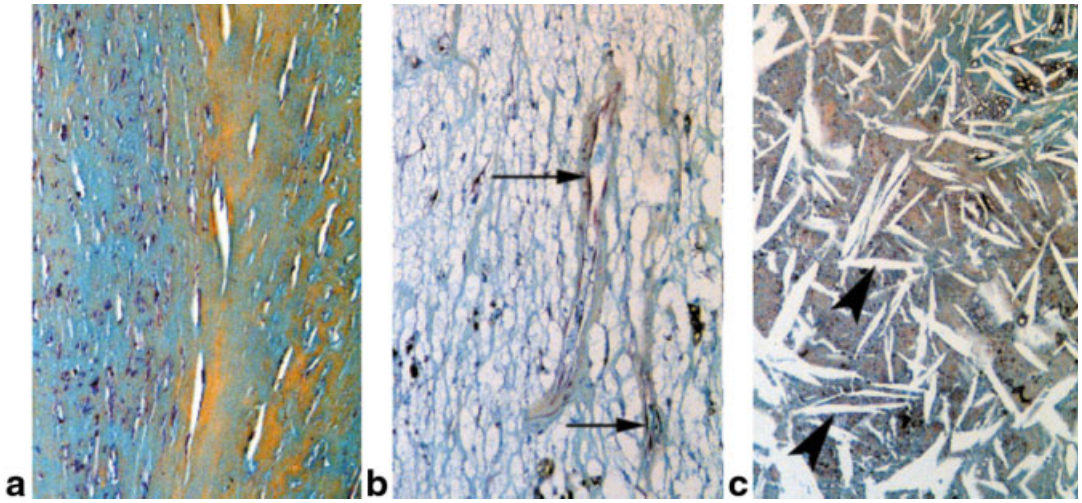

FIG. 2. Photomicrographs at 20× magnification demonstrating (**a**) fibrous tissue composed of spindle cells and dense collagen, (**b**) loose connective tissue with a reticular architecture and variable vascurlarity (arrows), and (**c**) the necrotic core of acellular amorphous material and frequent cholesterol crystals (arrowheads).

the training regions, retrospective comparison of the location of the training regions with the pathologist's tracings and the μCT verified that the training regions had been assigned to the correct tissue class. The choice of training regions probably has minimal impact on the classifier results, provided that the selection of these regions is consistent with the pathologist's interpretation of the histology and contains a sufficient number of pixels.

Truth regions for calcification were generated by thresholding the registered μCT images. The threshold was defined as the average signal intensity of the cortical bone-mimic minus three standard deviations (SDs). The values used for the average signal intensity and the SD were obtained by drawing a region of interest (ROI) within the bone-mimicking material on the μCT images. The use of a threshold based on the bone-mimic was justified because in a previous solid-state NMR spectroscopy study (14), calcified regions of atherosclerotic lesions were shown to be compositionally similar to cortical bone. Three SDs below the average signal intensity was chosen empirically because it ensured that all pixels within a calcified region were selected, without including any extraneous pixels.

Truth regions were compared on a pixel-by-pixel basis with the results of the minimum distance classifier. The results for all plaques were pooled to determine the overall sensitivity and specificity of the classifier for each plaque component. Sensitivity is defined as:

$$\frac{(\text{True Positives})}{(\text{True Positives} + \text{False Negatives})} \quad [1]$$

Therefore, for a given tissue class x, sensitivity was calculated as:

$$\frac{\text{No. pixels correctly labeled by the classifier as tissue } x}{\text{Total no. pixels labeled tissue } x \text{ as determined by gold standard method}}$$

Likewise, specificity is defined as:

$$\frac{(\text{True Negatives})}{(\text{True Negatives} + \text{False Positives})} \quad [2]$$

Consequently, for a given tissue class x, specificity was calculated as:

$$\frac{\text{No. of pixels correctly excluded from tissue } x \text{ by the classifier}}{\text{Total no. of pixels excluded from tissue } x \text{ as determined by gold standard method}}$$

The overall accuracy was calculated as:

$$\frac{\text{Total no. of pixels correctly labeled by the classifier}}{\text{Total no. of pixels analyzed}} \quad [3]$$

Reproducibility of Pathology Tracings

In this study, the gold standard for plaque constituents other than calcification was determined by manual tracings of the digitized histological images. Although a trained neuropathologist performed the segmentations, the decision to classify the plaque into various regions was subjective. To determine the reproducibility of these tracings, the pathologist retraced the digitized images of the same 10 plaques 6 weeks after the first tracing. The data from the 10 pairs of tracings were pooled for analysis. The percentage agreement for each plaque component was obtained by calculating the percentage of pixels that were labeled the same tissue type in both the first and second tracings. The variability between the two sets of tracings set an upper limit for the accuracy that could be expected from the classifier. The classifier accuracy was evaluated using the first set of tracings as the gold standard.

Table 2
Pixel-by-Pixel Comparison of Pathology Tracings*

2nd tracing	1st tracing				
	Fibrous	Necrotic core	Calcification	Loose CT	Total
Fibrous	**22059 (85.1)**	1037	0	181	23277
Necrotic core	1035	**33863 (96.9)**	0	0	34898
Calcification	0	0	**3000 (100)**	0	3000
Loose CT	2836	42	0	**2758 (93.8)**	5636
Total	25930	34942	3000	2939	66811

*The numbers on the diagonal (in bold) represent the number of pixels that were labeled by the pathologist as the same tissue type on both the first and second tracings of the digitized histological images. For a given plaque component, the numbers in parentheses represent the fraction of pixels that were labeled the same component in both tracings.

RESULTS

Reproducibility of Pathology Tracings

The pooled data comparing the two sets of tracings are summarized in Table 2. The overall agreement was 92.3%. The specific agreements were 85.1%, 96.9%, 100%, and 93.8% for fibrous tissue, necrotic core, calcification, and loose connective tissue, respectively. The percentage agreement for calcification was 100% because there was a defined criterion for the selection of calcified regions based on thresholding the μCT images, which eliminated the need for observer-dependent segmentation. Results for the other tissue components indicated that separation of necrotic core from fibrous tissue was very consistent between tracings; the largest source of error was separating fibrous tissue from loose connective tissue. As shown in Table 2, nearly 11% (2836/25930) of the pixels that were labeled fibrous in the first tracing were labeled loose connective tissue in the second tracing. Some amount of uncertainty in categorizing tissue as fibrous or loose connective tissue was expected because both types were present in some regions, and this uncertainty was reflected in the results. For example, if the second set of pathology tracings had been used as the gold standard instead of the first set, the agreement for loose connective tissue would have been 48.9%. This result indicated that perhaps in future studies these two tissue types should be combined; however, the absolute number of pixels for which there was disagreement was small. Despite this discrepancy, the overall intraobserver agreement was good, and visually the tracings agreed extremely well. We concluded that the pathologist's manual segmentation of carotid plaque constituents into the tissue classes used in this study was reproducible.

Training the Classifier

The average signal intensity values for each plaque component as a function of MR acquisition type are shown in Fig. 3. For a given MR contrast weighting, there was significant variability in the signal intensity of each plaque component, which is reflected in the large SD. Calcification was dark on all MR acquisitions, and thus was easily identified; however, there was significant overlap between the signal intensities for fibrous tissue and the necrotic core. Diffusion-weighted SE was the only contrast for which the SDs for fibrous tissue and necrosis did not overlap.

Accuracy of Carotid Plaque Classification

The results from all 10 plaques analyzed were pooled for final analysis, and the data are summarized in Table 3. A total of 72243 pixels were studied. The classification sensitivities for fibrous tissue, necrotic core, calcification, and loose connective tissue were 60.4%, 83.9%, 97.6%, and 65.2%, respectively. The corresponding classification specificities were 87.9%, 75.0%, 98.3%, and 94.9%, respectively. The largest source of error was confusion between fibrous tissue and the necrotic core. The overall accuracy of the classifier compared with histology, taking into account all pixels analyzed, was 73.5%.

Figure 4 illustrates the eight MR acquisitions and minimum distance classifier results for one plaque. The registered histology, pathologist's tracings, and corresponding μCT images are shown. In this case, the classifier correctly identified large regions of fibrous tissue, necrotic core, calcification, and loose connective tissue. In particular, the position and thickness of the fibrous cap separating the necrotic region from the lumen were in close agreement with the histology. Inspection of the eight MR acquisitions revealed that the only contrast by which the necrotic core was easily distinguished from the surrounding fibrous tissue was that of the diffusion-weighted sequence. This finding was in concordance with results shown in Fig. 3, and was a consistent observation across all 10 plaques in the data set.

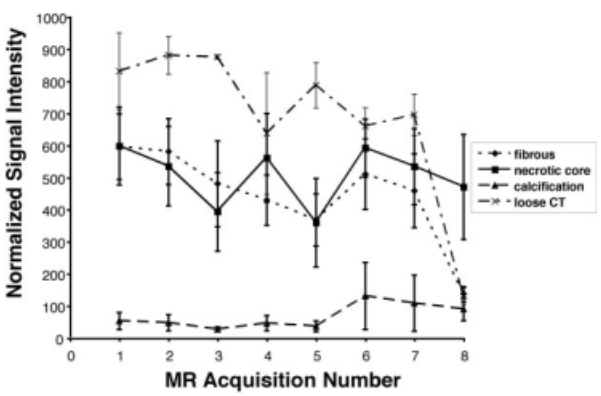

FIG. 3. Signal intensity of each plaque component as a function of MR contrast weighting. The MR acquisitions, in order, were: 1) PDw FSE, 2) partial T_2w FSE, 3) T_2w FSE, 4) T_1w FSE, 5) FIESTA, 6) T_1w SPGR, 7) T_1w SPGR with MT, and 8) Dw SE. Error bars represent the SD.

Table 3
Comparison of Classifier Results With Histology*

Classification by MR	Classification by Histology				
	Fibrous	Necrotic core	Calcification	Loose CT	Total
Unclassified	29 (0.1)	10 (0.03)	36 (1.2)	9 (0.3)	84
Fibrous	**18684 (60.4)**	3814 (11.0)	22 (0.7)	1164 (32.9)	23684
Necrotic core	9315 (30.1)	**29184 (83.9)**	14 (0.5)	39 (1.1)	38552
Calcification	1104 (3.6)	595 (1.7)	**2928 (97.6)**	22 (0.6)	4649
Loose CT	1779 (5.8)	1188 (3.4)	0.00 (0.0)	**2307 (65.2)**	5274
Total	30911	34791	3000	3541	72243

*Results of pixel-by-pixel comparison of minimum distance classifier results compared to the pathologist's segmentation of histology. The values on the diagonal (in bold) represent the number of correctly classified pixels for each tissue class. The numbers in parentheses are the corresponding percentages based on the total number of pixels in the truth region for that class. Pixels that fall in the unclassified category represent errors due to misregistration between MR images and histology.

An important feature of the classifier was the ability to select the subset of correct tissue classes present within a given plaque, given the tissue signatures of all possible components. Some plaques contained only fibrous tissue and necrotic regions, with no loose connective tissue or calcification (see Fig. 5). In this case, the fibrous cap overlying the necrotic core was well identified by the classifier, while the number of pixels classified as either calcification or loose connective tissue was minimal.

Atherosclerotic lesions are heterogeneous and often contain regions that consist of various tissue types, rather than just one component. These regions presented a segmentation challenge for both the classification algorithm and the pathologist, as shown in Fig. 6. For this lesion, the pathologist's two segmentations were not in good agreement; only 70.2% of the pixels were assigned to the same category on both the first and second tracings. Upon closer examination, it was noted that the region that was the source of disagreement between pathology segmentations contained loose connective tissue mixed with collagen. In the first tracing, the pathologist labeled this region as fibrous (green), while in the second tracing it was identified as loose connective tissue (blue). Because this area was a mixture of both tissue types, both classifications could be regarded as correct. The minimum distance classified image was intermediate between the two tracings, and ap-

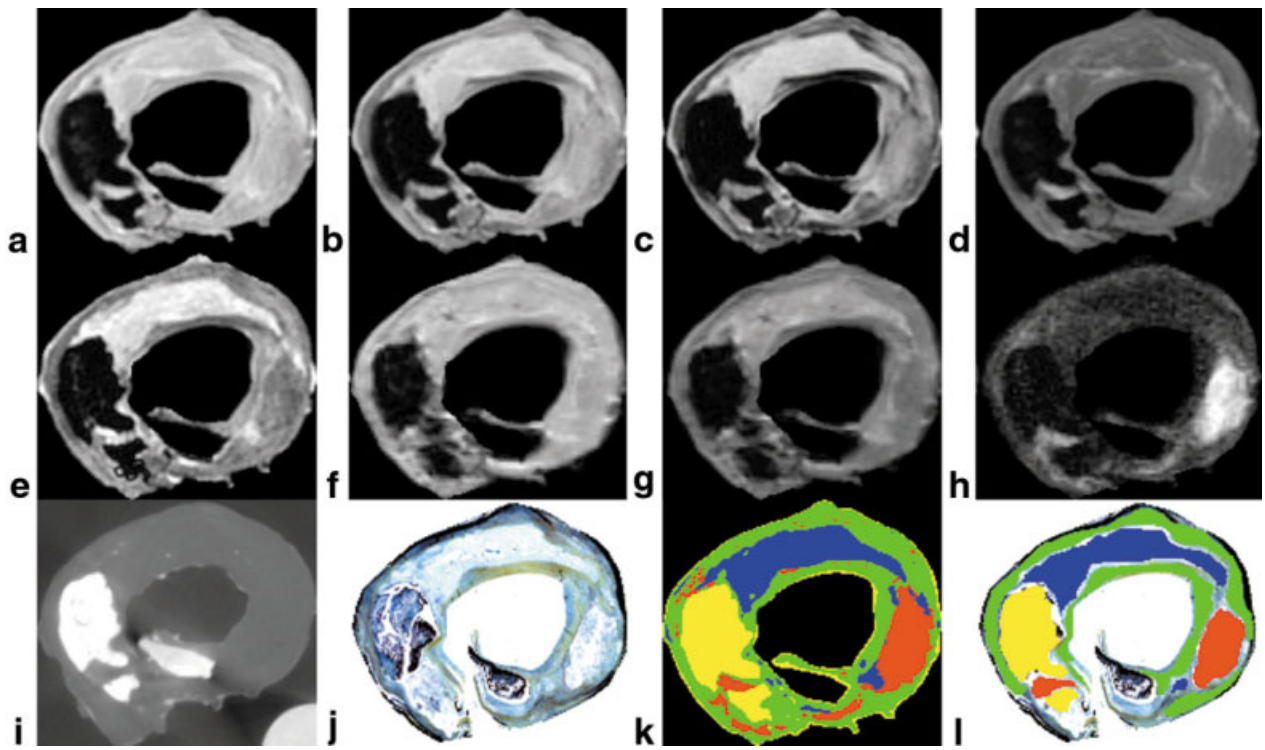

FIG. 4. Examples of typical images obtained with high-resolution carotid endarterectomy specimen protocol. Shown are PDw FSE (**a**), partial T_2w FSE (**b**), T_2w FSE (**c**), T_1w FSE (**d**), FIESTA (**e**), T_1w SPGR (**f**), T_1w SPGR with MT (**g**), and Dw SE (**h**). The corresponding μCT image (**i**) and registered histology (**j**) are also shown. The minimum distance classified image (**k**) agreed well with the pathologist's segmentation of histology (**l**). The overall accuracy for this plaque was 89%. **k** and **l:** fibrous tissue (green), necrotic core (red), calcification (yellow), and loose connective tissue (blue).

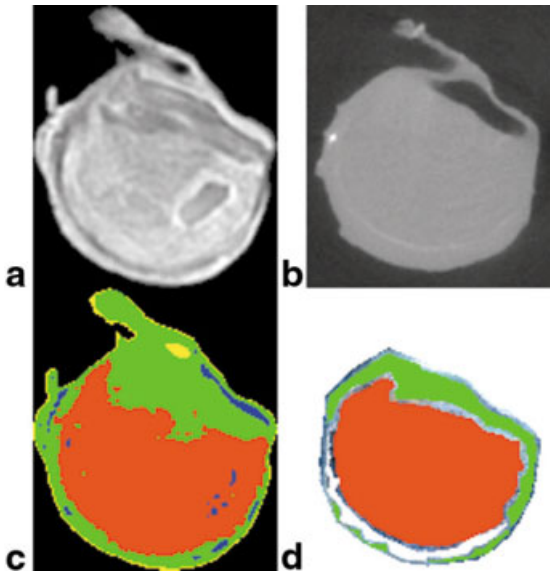

FIG. 5. This carotid plaque contained a necrotic core and fibrous tissue, but no calcification or loose connective tissue. The PDw MR image is shown in **a**; the corresponding μCT image (**b**) confirms the absence of calcification. The minimum distance classified image (**c**) correctly identified the necrotic core and fibrous cap, as verified by the pathologist's segmentation (overlaid on the registered histology) in **d**. Although only the PDw image is shown in this figure, all eight MR acquisitions were used as input for the minimum distance classifier. The overall accuracy of the classifier for this plaque was 90%. **c** and **d:** Fibrous tissue (green), necrotic core (red), calcification (yellow), and loose connective tissue (blue).

peared to be an accurate depiction of plaque morphology; however, a pixel-by-pixel comparison of the classifier results to the first pathology tracing (the gold standard) yielded an overall agreement of only 63.9%. This plaque illustrated the shortcomings of using histology as a gold standard for this type of study. In this regard, our method of evaluating the classification algorithm's performance may underestimate the classifier's accuracy. Overall, however, the pathologist's classifications were over 90% reproducible; this plaque represented the case with the most variability between pathology tracings.

DISCUSSION

This study demonstrates that multicontrast MRI can be used in conjunction with an automated classification algorithm to identify plaque constituents in endarterectomy specimens. Furthermore, the accuracy of the classifier has been validated in a more quantitative fashion than was previously reported. This was accomplished by registering histology with MR using a nonlinear warping algorithm, which then permitted a blinded comparison of the MR classifier results with a pathologist's segmentation of the histology on a pixel-by-pixel basis. This registration allowed for a more realistic and rigorous assessment of classifier accuracy because in addition to the presence or absence of a particular tissue type, the size and spatial distribution of the different plaque components were considered. This information is important for assessing plaque vulnerability. The thickness of the fibrous cap can distinguish a stable lesion from one that is prone to rupture (4), and some studies have indicated that the size of the necrotic core (also referred to as the lipid core, or lipid-rich necrotic core) may play a role in plaque stability. A large lipid core may put more stress on the fibrous cap (15,16). In addition, the proximity of calcification to the lipid core could introduce large gradients in stress and strain in that region (5), and calcified nodules near the lumen can serve as a nidus for thrombus formation (17).

Numerous MR pulse sequences have been advocated for imaging atherosclerotic plaque. Some of these sequences have been used in patients, while others remain experimental. We selected the eight MR contrast weightings used in this study after reviewing the literature and determining which contrast weightings had the potential to characterize plaque. Some contrast weightings have been shown to be valuable for analyzing plaque composition in vivo, and therefore were included in our study. In a small series of patients, T_2w SE images demonstrated the presence of fibrous tissue, calcification, and hemorrhage in carotid atherosclerotic plaques (18); however, in another series of

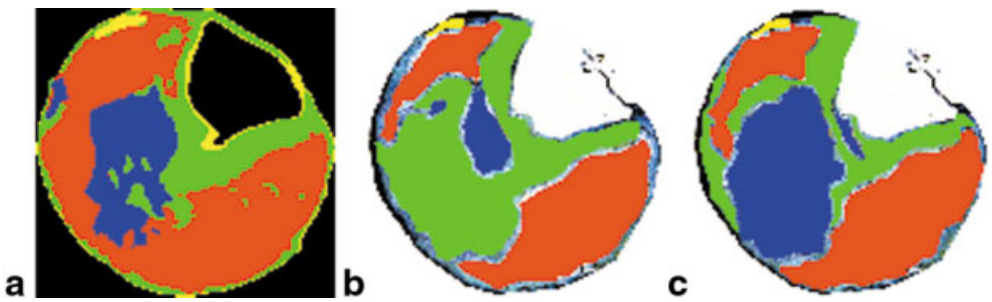

FIG. 6. Regions containing a mix of tissue types were often difficult to classify. In this case, the minimum distance classifier results (**a**) appeared to agree moderately well with the pathologist's segmentation of histology (**b**); however, pixel-by-pixel analysis yielded a low percentage accuracy (63.9%). This plaque showed the most variability between the pathologist's two tracings (**b** and **c**), only 70.2% of the pixels were labeled as the same plaque component both times. Regions of necrotic core (red) were well defined in both cases. The main source of disagreement was a section labeled fibrous (green) in **b**, which was labeled loose connective tissue (blue) at a later time (**c**). Retrospective analysis of this region revealed that it contained a mix of fibrous tissue and loose connective tissue, which made it difficult to classify both by automated and manual segmentation.

18 patients, Yuan et al. (8) found that T_1w FSE and TOF were more valuable contrasts for identifying lipid-rich necrotic core and intraplaque hemorrhage than either T_2w or PDw FSE images. TOF images can distinguish intact thick, fibrous caps from intact thin, ruptured caps (19), and the presence of plaque rupture detected using PDw, T_1w, T_2w FSE, and TOF images has been correlated with recent history of stroke or transient ischemic attack (20). The information obtained from the combination of PDw, T_1w, T_2w FSE, and TOF was also used in vivo to successfully categorize carotid plaque according to a modified American Heart Association classification scheme (9). Based on the results of these studies, PDw FSE, T_1w FSE, T_2w FSE, and T_1w SPGR were included in our imaging protocol. Our T_1w SPGR sequence and acquisition parameters were very similar to the TOF sequence used in the previously mentioned in vivo studies. Although fat saturation is often employed in the in vivo setting, its primary purpose is to suppress signal from the periadventitial fat, which is composed of mobile triglycerides. In the actual atherosclerotic lesion itself, the MR signal from plaque lipids (mainly cholesterol and its esters) is only 11% of the signal obtained from the water associated with the lipids in the necrotic core (21). Furthermore, Shinnar et al. (7) reported that using fat saturation for imaging endarterectomy specimens did not provide useful image contrast. For these reasons, we did not include fat saturation as one of the contrast weightings.

In ex vivo studies, several other pulse sequences have demonstrated value for identifying or discriminating between lesion components, including magnetization transfer (22,23), diffusion-weighted SE (7,24), and partial T_2w SE (7). In addition to these contrast weightings, we chose to include FIESTA, because a 3D image sequence with isotropic resolution may be necessary to characterize rapid changes in composition along the length of the plaque (25). Furthermore, we hypothesized that the FIESTA (also known as True FISP, balanced FFE, and SSFP) contrast mechanism, which is based on both T_1 and T_2 relaxation, would be useful for characterizing plaque because information on both T_1 and T_2 would be provided in one contrast weighting.

Although this study made use of ex vivo endarterectomy specimens, the behavior of the various plaque components on the different MR contrast weightings is in agreement with that reported for in vivo studies. Fibrous tissue displayed a moderate signal intensity on PDw, T_2w, and T_1w FSE, similar to that reported by Yuan et al. (8), who described dense, collagen-rich fibrous tissue as isointense relative to the sternocleidomastoid muscle on these three contrast weightings. In general, we found that the necrotic core was bright on T_1w FSE. Although the necrotic core was frequently dark on T_2w images, it was often similar in intensity to fibrous tissue. These findings are comparable to those described in vivo (8). Additionally, what we defined as loose connective tissue is analogous to what Yuan et al. (8) termed the "loose extracellular matrix" (8), and exhibits the same MR signal properties (i.e., bright signal intensity on both PDw and T_2w FSE, and relatively moderate signal on T_1w FSE). Finally, calcification was dark on all MR contrast weightings, as described previously (18,20).

It may not be necessary to use of all of the eight contrast weightings employed in our imaging protocol to adequately characterize plaque. A smaller subset may provide similar accuracy, or some of the contrast weightings may impart the same information. The methodology described herein can be applied to any number of MR contrast weightings. Future work will focus on determining the relative importance of each contrast weighting. From the results presented here, it appears that DWI is an important tool for separating fibrous tissue from the necrotic core. In our sample of 10 plaques, the necrotic core was usually bright on diffusion images, while fibrous tissue was almost always dark. Although most authors have advocated the use of DWI for identifying thrombus, the diffusion coefficient of the necrotic core is lower than that of fresh thrombus, 1-week-old thrombus, and organized thrombus (24). Consequently, the necrotic core would have higher signal intensity than thrombus on DW images. Furthermore, DW SE was the only contrast weighting on which the SDs for fibrous tissue and the necrotic core did not overlap.

Accurate image registration was of significant importance in this study. Both gold standards (μCT and histology) had to be registered to the MR images to facilitate the assessment of classifier accuracy. For μCT imaging, the specimens were transferred to a holder that ensured that the plaques were held in the same orientation as they had been when imaged with MR. This placement resulted in minimal distortion of the specimen and similar scan planes; therefore, linear image registration was quite accurate. Conversely, registration of the histology to the MR images could not have been done appropriately without the use of a nonlinear warping algorithm. Processing (e.g., dehydration and microtome sectioning) created distortions in the histological sections; however, we found that most of these distortions could be corrected within reason with the use of the Delaunay triangle method, provided that enough homologous points between MR images and histology had been selected. The greatest impediment to precise image registration was partial volume effects. The histological sections were 5μm thick, while the MR images were 200–1000 μm thick. Regions that were evident on histology were occasionally blurred on the MR images because of the larger slices. The error incurred by this misregistration was not quantified, but likely resulted in decreased classifier accuracy. The use of freon oil for specimen imaging created the possibility of another type of misregistration. Calcification near the edges of the plaque could be confused with either the lumen or the background outside the plaque. In practice, this was generally not a problem; however, any controversy that arose was resolved by corresponding μCT images that readily distinguished calcification from the background.

A possible limitation to this study was the choice of the minimum distance classifier to segment plaques. This classifier is fast and easy to implement; however, it does not make use of the covariance information and it depends only upon the mean positions of each tissue class (13). A more sophisticated classification algorithm could conceivably produce better results. Furthermore, in this study we classified each pixel individually, without considering the classification results for neighboring pixels. Incorporating information from neighboring pixels into the classification

algorithm would most likely produce more homogeneous regions in the classification map, with fewer isolated pixel labeling errors that might result from noisy data. One of the objectives of this study was to describe a framework for assessing classifier accuracy by registering histology with corresponding MR images, and in this context, the minimum distance classifier example can be regarded as proof of principle. The use of this framework will enable different classification algorithms to be compared in a quantitative fashion, so it can be determined whether the use of a more sophisticated segmentation algorithm does indeed result in increased classifier accuracy.

To further validate our use of the minimum distance classifier, we applied this algorithm to several additional endarterectomy specimens that were not included in the original data set described herein, and were not used to generate training data. The classification accuracies were similar, which suggests that once the classifier has been trained, it can be successfully applied to MR images of other plaques, provided that the image acquisition parameters are the same. This result holds promise for future in vivo plaque classification methods: histology would only be required for a small set of plaques for the purposes of collecting training data, and then the classification algorithm could be prospectively applied to new patient data.

The current concepts are very similar to those of Nair et al. (26), who used spectral analysis of backscattered intravascular ultrasound data to create tissue-specific maps of coronary artery plaques. As in our study, the classifier was trained using a subset of the data, and then applied to the remaining data; furthermore, as in our work, the classifier accuracy was assessed using Movat-stained sections warped to match the ultrasound images. Nair et al. (26) divided coronary plaques into four tissue classes: fibrous, calcified necrosis, calcification, and fibrolipidic regions. This choice of tissue classes is similar to the selection used in our study, in which plaques were segmented into fibrous tissue, necrotic core, calcification, or loose connective tissue. Therefore, it appears that most plaques can be adequately described with the use of only four tissue classes, which is a small enough number of classes to facilitate reproducible segmentation by a trained observer. The variation in histological interpretation is a limitation of all studies that address plaque composition, but ours is the first study to address and quantify this variability. Variability between the two sets of tracings by a trained observer set an upper limit for the accuracy that could be expected from the classifier.

CONCLUSIONS

In this work we described a method for acquiring multicontrast-weighted MR images of carotid plaque, and integrating the information to produce a single tissue-specific classification map. Furthermore, a technique for quantitatively assessing the accuracy of the classifier, based on registering MR images with histology and μCT images, was illustrated. The resulting pixel-by-pixel comparison assessed classifier accuracy in terms of identifying plaque components, as well as their spatial distribution and percentage area within the lesion. The variability in the gold standard interpretation of histology was also evaluated, which set an upper limit for the accuracy expected from the classifier. This methodology will provide a framework for comparing different classification algorithms, and determining which combination of MR contrasts will be the most valuable for imaging plaque in vivo.

ACKNOWLEDGMENTS

S.E.C. was the recipient of funding from the Canadian Institutes of Health Research (CIHR). B.K.R. receives salary support from the Barnett-Ivey-Heart and Stroke Foundation of Ontario Endowed Chair award. J.R.M. receives salary support from the MS Society of Canada Career Development Award, and the Alberta Heritage Foundation for Medical Research. In addition, the authors thank the Functional and Molecular Imaging Group of GE Medical Systems (specifically Mike Cole, Jennifer Dietrich, and Mike Thornton) for use of the micro-CT facilities, and the Department of Pathology, London Health Sciences Centre, for providing the endarterectomy specimens. We also thank Lei Dai for his help with data processing, and Yuteng Chen and Andrew Alejski for their assistance with the gradient coil insert.

REFERENCES

1. Lusis AJ. Atherosclerosis. Nature 2000;407:233–241.
2. Bassiouny HS, Sakaguchi Y, Mikucki SA, McKinsey JF, Piano G, Gewertz BL, Glagov S. Juxtalumenal location of plaque necrosis and neoformation in symptomatic carotid stenosis. J Vasc Surg 1997;26:585–594.
3. Seeger JM, Barratt E, Lawson GA, Klingman N. The relationship between carotid plaque composition, plaque morphology, and neurologic symptoms. J Surg Res 1995;58:330–336.
4. Golledge J, Greenhalgh RM, Davies AH. The symptomatic carotid plaque. Stroke 2000;31:774–781.
5. Glagov S, Bassiouny HS, Giddens DP, Zarins CK. Pathobiology of plaque modeling and complication. Surg Clin North Am 1995;75:545–556.
6. Serfaty JM, Chaabane L, Tabib A, Chevallier JM, Briguet A, Douek PC. Atherosclerotic plaques: classification and characterization with T_2-weighted high-spatial-resolution MR imaging—an in vitro study. Radiology 2001;219:403–410.
7. Shinnar M, Fallon JT, Wehrli S, Levin M, Dalmacy D, Fayad ZA, Badimon JJ, Harrington M, Harrington E, Fuster V. The diagnostic accuracy of ex vivo MRI for human atherosclerotic plaque characterization. Arterioscler Thromb Vasc Biol 1999;19:2756–2761.
8. Yuan C, Mitsumori LM, Ferguson MS, Polissar NL, Echelard D, Ortiz G, Small R, Davies JW, Kerwin WS, Hatsukami TS. In vivo accuracy of multispectral magnetic resonance imaging for identifying lipid-rich necrotic cores and intraplaque hemorrhage in advanced human carotid plaques. Circulation 2001;104:2051–2056.
9. Cai JM, Hatsukami TS, Ferguson MS, Small R, Polissar NL, Yuan C. Classification of human carotid atherosclerotic lesions with in vivo multicontrast magnetic resonance imaging. Circulation 2002;106:1368–1373.
10. Chu KC, Martin AJ, Rutt BK. Improved MR images of arterial specimens by submersion in trichlorotrifluoroethane. Magn Reson Med 1996;35:790–796.
11. White DR. Tissue substitutes in experimental radiation physics. Med Phys 1978;5:467–479.
12. Rasband W. ImageJ version 1.29n. National Institutes of Health, 2003. http://rsb.info.nih.gov/ij/
13. Richards JA. Remote sensing digital image analysis: an introduction. Berlin: Springer-Verlag; 1993.
14. Cho G, Hinton DP, Ackerman JL. Atherosclerotic plaque calcification is closely related to bone mineral: a solid state NMR spectroscopy study. In: Proceedings of the 10th Annual Meeting of ISMRM, Honolulu, 2002.
15. Huang H, Virmani R, Younis H, Burke AP, Kamm RD, Lee RT. The impact of calcification on the biomechanical stability of atherosclerotic plaques. Circulation 2001;103:1051–1056.

16. Richardson PD, Davies MJ, Born GV. Influence of plaque configuration and stress distribution on fissuring of coronary atherosclerotic plaques. Lancet 1989;2:941–944.
17. Virmani R, Kolodgie FD, Burke AP, Farb A, Schwartz SM. Lessons from sudden coronary death: a comprehensive morphological classification scheme for atherosclerotic lesions. Arterioscler Thromb Vasc Biol 2000;20:1262–1275.
18. Toussaint JF, LaMuraglia GM, Southern JF, Fuster V, Kantor HL. Magnetic resonance images lipid, fibrous, calcified, hemorrhagic, and thrombotic components of human atherosclerosis in vivo. Circulation 1996;94:932–938.
19. Hatsukami TS, Ross R, Polissar NL, Yuan C. Visualization of fibrous cap thickness and rupture in human atherosclerotic carotid plaque in vivo with high-resolution magnetic resonance imaging. Circulation 2000;102:959–964.
20. Yuan C, Zhang SX, Polissar NL, Echelard D, Ortiz G, Davis JW, Ellington E, Ferguson MS, Hatsukami TS. Identification of fibrous cap rupture with magnetic resonance imaging is highly associated with recent transient ischemic attack or stroke. Circulation 2002; 105:181–185.
21. Toussaint JF, Southern JF, Fuster V, Kantor HL. T_2-weighted contrast for NMR characterization of human atherosclerosis. Arterioscler Thromb Vasc Biol 1995;15:1533–1542.
22. Pachot-Clouard M, Vaufrey F, Darrasse L, Toussaint JF. Magnetization transfer characteristics in atherosclerotic plaque components assessed by adapted binomial preparation pulses. MAGMA 1998;7:9–15.
23. Rogers WJ, Prichard JW, Hu YL, Olson PR, Benckart DH, Kramer CM, Vido DA, Reichek N. Characterization of signal properties in atherosclerotic plaque components by intravascular MRI. Arterioscler Thromb Vasc Biol 2000;20:1824–1830.
24. Toussaint JF, Southern JF, Fuster V, Kantor HL. Water diffusion properties of human atherosclerosis and thrombosis measured by pulse field gradient nuclear magnetic resonance. Arterioscler Thromb Vasc Biol 1997;17:542–546.
25. Coombs BD, Rapp JH, Ursell PC, Reilly LM, Saloner D. Structure of plaque at carotid bifurcation: high-resolution MRI with histological correlation. Stroke 2001;32:2516–2521.
26. Nair A, Kuban BD, Tuzcu EM, Schoenhagen P, Nissen SE, Vince DG. Coronary plaque classification with intravascular ultrasound radiofrequency data analysis. Circulation 2002;106:2200–2206.